PCCP

RSC Publishing

PAPER

View Article Online
View Journal | View Issue

Cite this: *Phys. Chem. Chem. Phys.*, 2013, **15**, 3906

Photoinduced ultrafast dynamics of the triphenylamine-based organic sensitizer D35 on TiO_2, ZrO_2 and in acetonitrile

Kawon Oum,[a] Peter W. Lohse,[b] Johannes R. Klein,[a] Oliver Flender,[a] Mirko Scholz,[c] Anders Hagfeldt,[b] Gerrit Boschloo[b] and Thomas Lenzer*[a]

Received 17th November 2012,
Accepted 23rd January 2013

DOI: 10.1039/c3cp44095h

www.rsc.org/pccp

The relaxation dynamics of the dye D35 has been characterized by transient absorption spectroscopy in acetonitrile and on TiO_2 and ZrO_2 thin films. In acetonitrile, upon photoexcitation of the dye *via* the $S_0 \rightarrow S_1$ transition, we observed ultrafast solvation dynamics with subpicosecond time constants. Subsequent decay of the S_1 excited state absorption (ESA) band with a 7.1 ps time constant is tentatively assigned to structural relaxation in the excited state, and a spectral decay with 203 ps time constant results from internal conversion (IC) back to S_0. On TiO_2, we observed fast (<90 fs) electron injection from the S_1 state of D35 into the TiO_2 conduction band, followed by a biphasic dynamics arising from changes in a transient Stark field at the interface, with time constants of 0.8 and 12 ps, resulting in a characteristic blue-shift of the $S_0 \rightarrow S_1$ absorption band. Several processes can contribute to this spectral shift: (i) photoexcitation induces immediate formation of $D35^{\bullet+}$ radical cations, which initially form electron–cation complexes; (ii) dissociation of these complexes generates mobile electrons, and when they start diffusing in the mesoporous TiO_2, the local electrostatic field may change; (iii) this may trigger the reorientation of D35 molecules in the changing electric field. A slower spectral decay on a nanosecond timescale is interpreted as a reduction of the local Stark field, as mobile electrons move deeper into TiO_2 and are progressively screened. Multiexponential electron–cation recombination occurs on much longer timescales, with time constants of 30 μs, 170 μs and 1.4 ms. For D35 adsorbed on ZrO_2, there is no clear evidence for a transient Stark shift, which suggests that initially formed cation–electron (trap state) complexes do not dissociate to form mobile conduction band electrons. Multiexponential decay with time constants of 4, 35, and 550 ps is assigned to recombination between cations and trapped electrons, and also to a fraction of D35 molecules in S_1 which decay by IC to S_0. Differential steady-state absorption spectra of $D35^{\bullet+}$ in acetonitrile and dichloromethane provide access to the complete $D_0 \rightarrow D_1$ band. The absorption spectra of D35 and $D35^{\bullet+}$ are well described by TDDFT calculations employing the MPW1K functional.

1. Introduction

Organic chromophores employing triphenylamine-based donor substituents have recently attracted considerable attention as promising sensitizers for dye-sensitized solar cells (DSCs).[1–15] Specifically, a series of such dyes was developed (termed D29, D35 and D37), which feature *p*-substitution with additional functionalized phenyl groups at two of the phenyls of the triphenylamine unit and an electron-withdrawing combination of a thiophene group, conjugated with a cyanoacrylic acid residue at the third phenyl ring.[7] Fig. 1 shows the chemical structure of D35, which contains *o*- and *p*-substitution with a total of four butoxy groups. In DSCs, this dye shows a remarkably large open-circuit voltage, which is ascribed to the insulating properties of the butoxy chains.[6,7] In addition, it was found that the four butoxy substituents provide an anti-aggregation functionality, and thus render the addition of coadsorbents such as chenodeoxycholic acid superfluous.[16]

So far, the photoinduced dynamics of D35 have been mainly investigated on longer timescales, where the dye was attached

[a] *Universität Siegen, Physikalische Chemie, Adolf-Reichwein-Str. 2, 57076 Siegen, Germany. E-mail: lenzer@chemie.uni-siegen.de; Fax: +49 271 740 2805; Tel: +49 271 740 2803*
[b] *Department of Chemistry-Ångström Laboratory, Uppsala University, Box 523, SE 751 20 Uppsala, Sweden*
[c] *Max-Planck-Institut für biophysikalische Chemie, Am Fassberg 11, 37077 Göttingen, Germany*

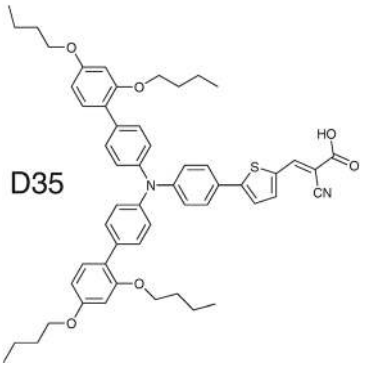

Fig. 1 Chemical structure of the triphenylamine-based dye D35.

to mesoporous TiO_2 electrodes and in contact with electrolyte solutions with and without a redox partner.[17] Notably, in photoinduced absorption (PIA) spectra a pronounced ''local Stark effect'' was observed for the D35–TiO_2 system.[6,17–19] This effect arises from the local electric field between the dye cations and injected electrons (or electrolyte counter cations and injected electrons after dye cation regeneration).[20–22] It acts on D35 molecules in the ground electronic state and leads to a blue-shift of the $S_0 \rightarrow S_1$ absorption spectrum. It also influences the spectral properties of other species present on the surface, *e.g.* the absorption spectra of the cations generated after photoinjection. While in the aforementioned studies the local Stark effect has been analyzed under ''pseudo steady-state'' conditions in PIA spectra and on the several nanoseconds to milliseconds time range in selected transient absorption spectra, its characterization on ultrafast timescales is largely missing. One exception is a previous study of the indoline dye D149 attached to electrodeposited ZnO thin films, where the local Stark effect was characterized on timescales from femto- to several hundred picoseconds.[23] A transient build-up of the Stark shift with a time constant of *ca.* 20 ps was observed, which was assigned to the break-up and separation of initially formed $D149^{\bullet+}$–electron complexes, and possibly also reorientational motion of ground-state D149 in the local electric field. Unfortunately, in those experiments the inherent chemical instability of D149 on TiO_2 did not permit a detailed study of the Stark shift for this particular mesoporous semiconductor oxide surface.

In the current study, we provide a detailed comparison of the ultrafast dynamics of the D35 dye on mesoporous TiO_2, mesoporous ZrO_2 (having a large band gap) and in acetonitrile solution. We identify characteristic timescales of the different intramolecular and intermolecular relaxation pathways of the photoexcited dye, as well as time constants for the build-up of the local Stark effect for the D35–TiO_2 system. We will show that the influence of the local Stark effect on the transient spectra is quite drastic, similar to the previous study for D149–ZnO.[23] Therefore, this finding has considerable consequences for the interpretation of transient spectral changes in any pump–probe experiment on dye-sensitized mesoporous semiconductor oxide surfaces.

2. Experimental

2.1 Preparation of thin films and solutions

For preparation of the TiO_2 thin films, 1.2 g of TiO_2 paste (Dyesol DSL 90T) were thoroughly mixed with 600 mg of isopropanol and treated in an ultrasonic bath for 20 minutes. The paste was then doctor bladed on 1 mm thick microscope slides. After sintering at 450 °C for 30 minutes and slowly cooling down overnight, highly transparent films with a thickness of 2–3 μm were obtained. For sensitization, films were placed in a 0.2 mM solution of D35 in acetonitrile for 5–10 minutes, then rinsed with fresh acetonitrile to remove unattached D35, and solvent was removed under a stream of dry nitrogen gas or in a vacuum desiccator. An analogous procedure was applied for the ZrO_2 films. The typical optical density (OD) of the D35-sensitized films was in the range 0.6–1.2 at the absorption maximum of the $S_0 \rightarrow S_1$ band. Addition of a co-adsorbent for avoiding aggregation is not required in the case of D35, as shown previously.[16]

We note that the steady-state absorption spectrum for D35 in acetonitrile shifted to the blue by 56 nm, when the concentration was below *ca.* 10^{-5} M. We ascribe this behavior to deprotonation of D35 by the residual water in the solvent (*ca.* 340 ppm). Such deprotonation was avoided by adding a very small amount of acetic acid just large enough to shift the acid–base equilibrium to the acid side: this approach had no impact on the spectroscopic results, as was tested against D35 solutions at higher concentration (2×10^{-4} M), where deprotonation was negligible.

2.2 Pump–supercontinuum probe (PSCP) spectroscopy

Ultrafast PSCP[24] experiments were carried out in acetonitrile and on TiO_2 and ZrO_2 thin films in contact with air using our setup described previously.[23,25–27] For the experiments in acetonitrile, a flow cell (1 mm path length) with a 200 μm thick quartz entrance window was used. Thin films were mounted on an *x*/*y* translation stage and moved in a plane perpendicular to the probe light path to expose a fresh spot for every laser shot. Samples were excited using a NOPA (λ_{pump} in the range 510–520 nm, beam diameter at the sample *ca.* 100 μm, energy *ca.* 1.5 μJ per pulse) and probed by a supercontinuum (370–770 nm, beam diameter at the sample *ca.* 50 μm), which was generated in a CaF_2 plate (thickness 1 mm). The pump–probe intensity cross-correlation time was *ca.* 130 fs for the experiments in acetonitrile (determined from the ultrafast solvent response), and *ca.* 90 fs for the thin film experiments (as obtained from the response of a TiO_2 thin film without D35). The accuracy in the determination of time zero was *ca.* 20 fs. No significant signs of photoinduced degradation of the sample were observed during the experiments.

2.3 Transient absorption spectroscopy on longer timescales

D35–TiO_2 samples were excited at the 10 Hz repetition rate using an optical parametric oscillator (OPO, GWU basiScan, FWHM 4 ns), which was pumped by the third harmonic of a Nd:YAG laser (Continuum Surelite I-20). Transient absorption

was probed using light from a high-pressure Hg/Xe lamp (Ushio UXM-200H, 200 W). Direct band-gap excitation of the TiO_2 was suppressed by using a 2 mm GG 435 edge filter (Schott) in front of the lamp. Transient absorption signals were detected by a combination of a double prism monochromator (Zeiss MM 12) and a photomultiplier tube (Hamamatsu 1P28). The output of the PMT was fed into a digital storage oscilloscope (Tektronix TDS 540A). The time resolution of this setup was *ca.* 500 ns. Typically 5000 laser shots were averaged for obtaining the transient absorption traces. The beam diameter of the laser at the sample was *ca.* 15 mm, and the excitation pulse fluence *ca.* 3 mJ cm^{-2}.

2.4 Spectroelectrochemistry

Spectroelectrochemistry of D35 was performed in nitrogen-purged acetonitrile and dichloromethane (DCM) solutions. This was done in the presence of tetrabutylammonium perchlorate (100 mM) as a supporting electrolyte. The details of the setup were described previously: we used an optically transparent thin-layer electrochemical (OTTLE) cell with 200 μm path length,[28] connected to a potentiostat (Metrohm Autolab PGSTAT 101).[23] The cell consists of a Pt-disk working electrode, a Pt-gauze auxiliary electrode and an Ag-wire as a pseudoreference electrode. A Varian Cary 5000 spectrometer was employed to record absorption spectra over the spectral range 200–2000 nm.

Spectroelectrochemistry of D35 on a TiO_2 thin film was carried out using a three-electrode setup connected to a CH Instruments 660 potentiostat.[29] The D35-coated nanoporous TiO_2 film on a fluorine doped tin oxide (FTO) glass substrate served as the working electrode, a Pt wire was used as the counter-electrode, and an Ag wire as the pseudoreference electrode. The electrodes were immersed in an electrolyte consisting of 100 mM tetrabutylammonium perchlorate in acetonitrile. Spectra were collected using an Ocean Optics HR-2000 spectrometer *via* fiber optics.

2.5 Calculations

DFT/TDDFT calculations were carried out to assign the electronic transitions observed in the steady-state absorption spectra of neutral D35 and the $D35^{\bullet+}$ radical cation difference absorption spectra from spectroelectrochemistry and the PSCP experiments. The equilibrium structures of D35 (S_0) and $D35^{\bullet+}$ (D_0) were optimized using the B3LYP functional[30] and a 6-31G(d) basis set. Time-dependent density functional theory (TDDFT)[31,32] was applied to these geometries for calculating the lowest 5 singlet (neutral D35) and lowest 20 doublet ($D35^{\bullet+}$) excited electronic states at vertical excitation using MPW1K[33] and B3LYP functionals in combination with a 6-31+G(d) basis set. Calculations were carried out using the Gaussian 09 package.[34] Detachment–attachment densities[35] were calculated using the Q-Chem 3.0 package.[36]

3. Results and discussion

3.1 Steady-state absorption spectra of D35 and $D35^{\bullet+}$

Steady-state absorption and emission spectra of neutral D35 are illustrated in Fig. 2(A). The spectrum in acetonitrile (black)

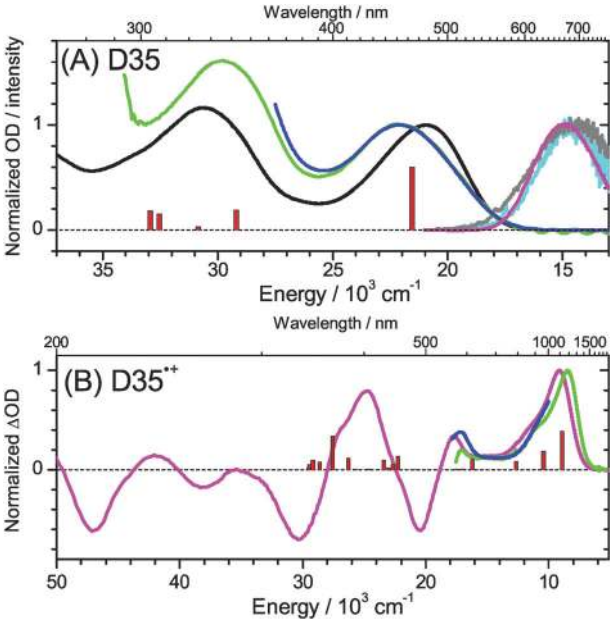

Fig. 2 (A) Steady-state absorption spectra of D35 in acetonitrile (black), on ZrO_2 (green) and on TiO_2 (blue); fluorescence spectra of D35 in acetonitrile (grey), on ZrO_2 (magenta), and on TiO_2 (light blue). (B) Differential steady-state absorption spectra of the $D35^{\bullet+}$ radical cation in acetonitrile (magenta), dichloromethane (green), and on TiO_2 (blue). The red columns in (A) and (B) represent stick spectra of the first 5 and 20 vertical electronic transitions of D35 and $D35^{\bullet+}$, respectively, obtained from TDDFT calculations (MPW1K functional), where the amplitudes are proportional to the oscillator strengths (Table 1).

shows two prominent bands centered at 477 nm and 327 nm, which are assigned to the $S_0 \rightarrow S_1$ and $S_0 \rightarrow S_2$–S_5 transitions, respectively.[7] The fluorescence band (grey) peaks at 669 nm, resulting in a large Stokes shift of 6540 cm^{-1}, which indicates formation of strong charge transfer character in the emitting state. This Stokes shift in acetonitrile is larger than that in DCM (4800 cm^{-1}).[9] The peaks of the $S_0 \rightarrow S_1$ absorption transition of D35 on ZrO_2 (green) and TiO_2 (blue) are broadened and blue-shifted by *ca.* 25 nm relative to acetonitrile. Due to the fairly large band gap of ZrO_2 (*ca.* 5 eV), the $S_0 \rightarrow S_2$–S_5 band is also clearly visible and in this case red-shifted by *ca.* 10 nm compared to acetonitrile. The considerably larger ratio OD_{max}(336 nm)/OD_{max}(450 nm) of the two main peaks in the case of ZrO_2 (green) suggests that an overlapping charge transfer band is responsible for the additional absorption in this spectral region, as observed previously for systems such as catechol–ZrO_2.[37] The peak of the fluorescence spectrum of D35 on ZrO_2 (magenta) is located at 658 nm and slightly shifted to the blue compared to acetonitrile. Still, the Stokes shift amounts to 7250 cm^{-1} and is larger than that in acetonitrile. Considering the dipolar character of the D35 molecules, this behavior may originate from efficient stabilization of D35 in the S_1 state by the surrounding D35 molecules in the ground state on the surface (*i.e.* qualitatively similar to dipolar solvation in polar organic solvents). In addition, energy transfer to the energetically lowest site in aggregated dye complexes on the surface might lead to substantially red-shifted emission.

The peak of the fluorescence spectrum of TiO_2 (light blue line) is located at 669 nm and is thus slightly more red-shifted than in the case of ZrO_2. We note that the integrated fluorescence intensity is about 18 times weaker than that for D35–ZrO_2.

Differential steady-state absorption spectra of the $D35^{\bullet+}$ radical cation are shown in Fig. 2(B). The spectrum in acetonitrile (magenta) covers the wavelength range 200–2000 nm and considerably extends the spectral range compared to previous studies.[18] Negative-going features correspond to the bleach of electrochemically converted D35 neutrals, resembling the inverted steady-state absorption spectrum. Here we present radical cation spectra over a wide range of wavelengths including the complete $D_0 \rightarrow D_1$ absorption band, which peaks in the near IR region at 1097 nm. Additional absorption peaks are visible at 565, 404 and 238 nm. Assignments of the individual bands will be discussed further below together with results from our accompanying DFT/TDDFT calculations. Differential absorption spectra of $D35^{\bullet+}$ were also recorded in DCM. Whereas in acetonitrile two clearly separated oxidation steps were observed in the cyclic voltammogram at 0.92 and 1.25 V (*vs.* the Ag pseudoreference electrode), in DCM only a gradual increase was found in this range. We believe that side reactions occur in DCM. This is supported by the fact that upon normalization of the spectra with respect to the maximum of the $D_0 \rightarrow D_1$ absorption band, the bleach of D35 in DCM is enhanced by about a factor of two compared to acetonitrile and additional absorption emerges below 450 nm. Therefore, in Fig. 2(B), the spectrum in DCM is only shown down to 570 nm, where there appear to be no spectral contributions from side reaction products. In DCM the peak ($D_0 \rightarrow D_1$) is located at 1182 nm.

A preliminary $D35^{\bullet+}$ spectrum on TiO_2 is also shown as a blue line in Fig. 2(B) over a restricted wavelength range. It is consistent with the one previously reported,[18] and appears to be only slightly red-shifted relative to that in acetonitrile (*ca.* 400 cm^{-1}). Knowledge of the radical cation spectrum is helpful in the interpretation of electron injection processes in the PSCP experiments reported below.

3.2 DFT/TDDFT calculations for D35 and $D35^{\bullet+}$

We carried out complementary DFT/TDDFT calculations in order to characterize the electronic transitions observed in the steady-state spectra of Fig. 2. Results are summarized in Table 1. Previously, we found very good agreement between the calculated and experimental electronic transitions for the indoline radical cation $D149^{\bullet+}$, when the MPW1K functional was employed.[23] In the current study, we used the same approach for both the $D35^{\bullet+}$ radical cation and neutral D35, and results for the first 20 (cation) and 5 (neutral) electronic transitions are included in Fig. 2 as red columns. In (A), the position of the $S_0 \rightarrow S_1$ band in the steady-state absorption spectrum of D35 is well reproduced as is the clear energy gap to the higher electronic states. According to the calculations, the broad band centered at 327 nm is dominated by the three transitions $S_0 \rightarrow S_2$, $S_0 \rightarrow S_4$ and $S_0 \rightarrow S_5$ with similar oscillator strength, with an additional weaker contribution of $S_0 \rightarrow S_3$. We note that previous calculations for neutral D35 employing the B3LYP functional are substantially red-shifted,[7] and we confirmed this by our own calculations, which are also summarized in Table 1.

Table 1 Results of DFT/TDDFT calculations for D35 and the $D35^{\bullet+}$ radical cation: wavelengths of the vertical electronic transitions using B3LYP and MPW1K functionals, in the latter case including oscillator strengths *f*

Transition	λ/nm (B3LYP)	λ/nm (MPW1K)	*f* (MPW1K)
D35			
$S_0 \rightarrow S_1$	597	464	1.18
$S_0 \rightarrow S_2$	456	343	0.38
$S_0 \rightarrow S_3$	428	324	0.06
$S_0 \rightarrow S_4$	372	307	0.31
$S_0 \rightarrow S_5$	360	304	0.36
$D35^{\bullet+}$			
$D_0 \rightarrow D_1$	1354	1124	0.55
$D_0 \rightarrow D_2$	1128	958	0.27
$D_0 \rightarrow D_3$	867	790	0.12
$D_0 \rightarrow D_4$	840	617	0.14
$D_0 \rightarrow D_5$	778	590	0.01
$D_0 \rightarrow D_6$	641	573	0.01
$D_0 \rightarrow D_7$	574	508	0.00
$D_0 \rightarrow D_8$	546	482	0.00
$D_0 \rightarrow D_9$	510	449	0.20
$D_0 \rightarrow D_{10}$	496	441	0.08
$D_0 \rightarrow D_{11}$	492	434	0.03
$D_0 \rightarrow D_{12}$	487	427	0.14
$D_0 \rightarrow D_{13}$	463	406	0.01
$D_0 \rightarrow D_{14}$	460	389	0.01
$D_0 \rightarrow D_{15}$	457	380	0.17
$D_0 \rightarrow D_{16}$	425	363	0.48
$D_0 \rightarrow D_{17}$	412	350	0.11
$D_0 \rightarrow D_{18}$	411	343	0.14
$D_0 \rightarrow D_{19}$	406	340	0.07
$D_0 \rightarrow D_{20}$	393	339	0.03

Detachment–attachment electron density plots[35] for the $S_0 \rightarrow S_1$ and $S_0 \rightarrow S_2$ transitions are depicted in Fig. 3. According to the calculations employing the MPW1K functional, the former one is predominantly HOMO → LUMO in character

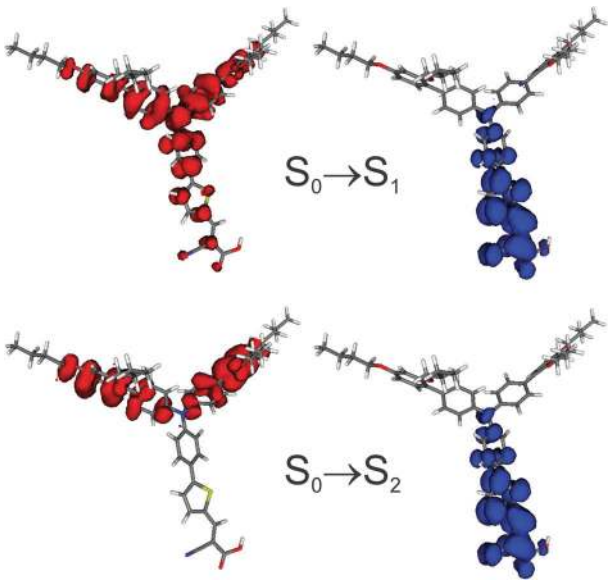

Fig. 3 Detachment (red) and attachment (blue) electron densities of the $S_0 \rightarrow S_1$ (top) and $S_0 \rightarrow S_2$ (bottom) transitions of neutral D35 (B3LYP).

(with some contributions from HOMO − 2 → LUMO and HOMO → LUMO + 1), while the latter one is governed by HOMO − 2 → LUMO (with additional contributions of HOMO − 3 → LUMO, HOMO → LUMO and HOMO − 5 → LUMO). For both transitions substantial intramolecular charge transfer is found: electron density is shifted from the substituted triphenylamine group toward the thiophene–cyanoacrylic acid moiety.[7] This is in agreement with the change in dipole moment, which, *e.g.*, increases from 15.0 (14.4) D to 33.7 (38.6) D in the case of the $S_0 \rightarrow S_1$ transition, based on calculations employing the MPW1K (B3LYP) functional. In fact, such deliberate design of the electronic properties of solar cell dyes is believed to allow for facile electron injection into the semiconductor oxide surface by moving electron density toward the carboxylic anchor group and therefore closer to the surface.[4,7]

For the $D35^{\bullet+}$ radical cation, the calculations employing the MPW1K functional describe the complete spectrum very well. The near IR band is dominated by the $D_0 \rightarrow D_1$ peak and the shoulder to the blue is due to the $D_0 \rightarrow D_2$ and $D_0 \rightarrow D_3$ transitions. The small band at 565 nm likely arises from the $D_0 \rightarrow D_4$ transition. Toward lower wavelength we find contributions from several transitions ($D_0 \rightarrow D_9/D_{10}/D_{12}/D_{15}$–$D_{19}$), which are responsible for the appearance of the prominent broad absorption feature peaking at 404 nm, which is superimposed on the bleach of neutral ground state D35.

We conclude that the MPW1K functional, with a larger amount of Hartree–Fock exchange, obviously leads to a better description of the excited electronic states of both D35 and $D35^{\bullet+}$ than B3LYP does. This is in agreement with previous findings for a series of larger organic solar cell dyes having substantial charge transfer character.[33]

3.3 Transient absorption spectra of D35 in acetonitrile

Fig. 4 depicts transient absorption spectra of D35 in acetonitrile after excitation at 512 nm. In panel (A), the development at early times is shown. Up to 50 fs, one observes the appearance of ground state bleach (GSB), which is centered at *ca.* 500 nm. At the same time, superimposed excited state absorption (ESA) of the S_1 state emerges below 450 nm and above 530 nm. With progressing time, the GSB feature becomes less pronounced and slightly shifts to the blue (peak at 480 nm). At the same time the ESA at around 570 nm strongly grows. By 150 fs pump–probe delay, the $S_1 \rightarrow S_0$ stimulated emission (SE) band centered at *ca.* 670 nm is clearly visible. In panel (B) there is further growth of the ESA band and the SE band shifts further to the red. This movement is practically completed by *ca.* 1 ps. The transient changes in the panels (A) and (B) are consistent with solvation dynamics of acetonitrile in response to the substantial dipole moment change of D35 upon $S_0 \rightarrow S_1$ excitation: the SE feature shifts from 670 nm to 710 nm and also gains amplitude. Its band minimum approaches that of the steady-state SE spectrum, which is shown as a dashed orange line in panel (D). Note that the rise of the ESA band at 570 nm takes place on the same timescale. This is likely due to a superimposed part of the SE band, which also shifts to the red. The interpretation of the spectral dynamics in that region

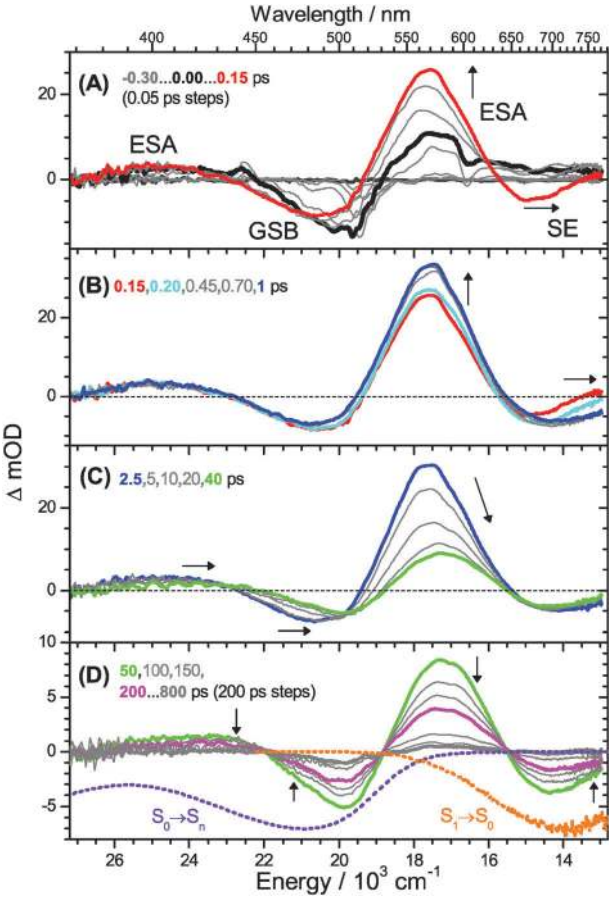

Fig. 4 Transient PSCP spectra of D35 in acetonitrile. Laser excitation at 512 nm. The dashed violet and orange lines in the bottom panel represent a scaled and inverted steady-state absorption spectrum and a scaled steady-state stimulated emission spectrum. The arrows depict band movements.

is further supported by the fact that the band integral above 510 nm is approximately conserved. These solvation dynamics are well described by known parameters for acetonitrile solvation processes (time constants of 89 and 630 fs).[38] In agreement with this interpretation, the ESA band below 420 nm stays essentially unchanged during this process, because there is no SE in this region, and the position of the ESA band is apparently less sensitive to solvation, as has been also observed for *N*-methyl-6-quinolone in water.[39] We note that the spectral development of D35 in acetonitrile on this timescale closely resembles that of the indoline dye D149 in the same solvent, as previously demonstrated by us.[25] In acetonitrile, such a behavior is expected, because solvent relaxation is much faster than the rotational diffusion of the solute, compare *e.g.* the experiments by Sajadi, Ernsting and co-workers where this was demonstrated for a range of solute–water systems.[40]

Additional dynamics take place between 2.5 and 40 ps (see panel (C)). The large ESA band at 560 nm and the smaller SE band at 700 nm decrease considerably, and the former shifts 20 nm to the red. At the same time, the GSB and the weak ESA band at lower wavelengths also shift to the red and exhibit changes in amplitude. From the global analysis we obtain a

time constant of 7.1 ps. The underlying process is not entirely clear. Photoisomerization can be ruled out, because of several reasons: in panel (D) at long times the bands have almost completely decayed by 800 ps, meaning that the original S_0 population has been recovered. Also, in the case of an isomerization, one would expect just a simple shift of the ESA band without a drastic loss in amplitude, because only a minor spectral modification is involved (compare *e.g.* the case of the indoline dye D149).[25] Moreover, for such a large molecule, isomerization should be very slow, because the excess energy is distributed over many vibrational modes, so it will take considerable time until enough energy ends up in the "critical mode" driving the isomerization. Finally, very recent STM experiments suggest that the yield of photoinduced isomerization of D35 is very low (< 0.3%), at least on a TiO_2 surface.[41] We therefore believe that the 7.1 ps dynamics are due to a change in electronic character of D35, *e.g.* due to structural relaxation in the excited state after Franck–Condon excitation. The change in amplitude would then reflect a reduction of oscillator strength for absorption and emission of the structurally relaxed species.

Panel (D) shows the development on long timescales from 50 ps onwards. There are four isosbestic points at *ca.* 380, 455, 530 and 645 nm, and all bands uniformly decay with a time constant of 203 ps. This process is assigned to internal conversion back to S_0.

Selected kinetic traces at three representative probe wavelengths are shown in Fig. 5(A), including fit results from a global analysis procedure using the simple kinetic model $S_1 \rightarrow S_0$ with a time-dependent spectrum for the S_1 state.[42,43] In the transient at 522 nm (red), $S_0 \rightarrow S_1$ GSB and $S_1 \rightarrow S_0$ SE appear first. These then quickly change into $S_1 \rightarrow S_n$ ESA due to sub-picosecond solvation dynamics (the SE shifts to longer wavelengths, and then ESA overwhelms the underlying GSB contribution). Afterwards the ESA decays (structural relaxation with a time constant of 7.1 ps), so that the GSB contribution dominates again. The transient eventually decays to zero (IC time constant: 203 ps). At the probe wavelength of 611 nm (green) we observe an immediate rise in $S_1 \rightarrow S_n$ ESA, with a curvature at very early times, which again signals solvation dynamics due to the superimposed transient red-shift of the SE contribution. The ESA then decays in a biexponential fashion (structural relaxation and subsequent IC). At 750 nm (blue), first $S_1 \rightarrow S_n$ ESA forms, which quickly converts to $S_1 \rightarrow S_0$ SE, because of the transient red-shift of the SE band. The SE then decays in a biexponential fashion due to structural relaxation and IC.

3.4 Transient absorption of D35 on TiO_2

Fig. 6 shows transient absorption spectra of D35 on TiO_2 after excitation at 518 nm. In panel (A), the spectral development at very early times is depicted. It is characterized by the formation of a GSB band centered at *ca.* 490 nm and two absorption bands at 410 and 590 nm, respectively. The large (40 nm) difference between the minimum of the GSB and the minimum of the inverted steady-state absorption spectrum of D35

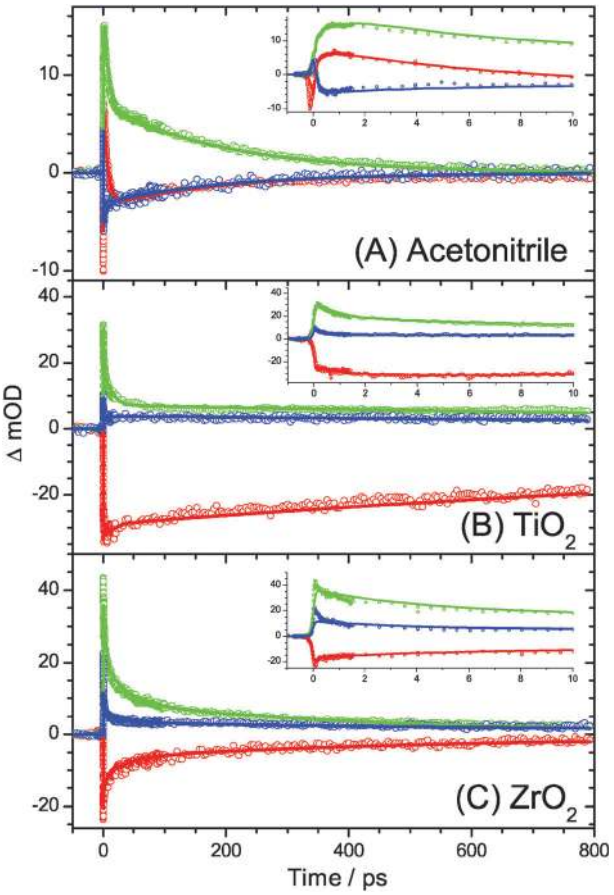

Fig. 5 Selected kinetic traces and global analysis results for D35 in (A) acetonitrile, (B) on TiO_2 and (C) on ZrO_2. Probe wavelengths: 522 nm (red), 611 nm (green) and 750 nm (blue). The insets show magnifications at early times.

(dashed orange line in panel (C)) suggests that electron injection has already largely occurred within the time resolution of this experiment (*ca.* 90 fs). The absorption above *ca.* 560 nm and below 440 nm is dominated by $D_0 \rightarrow D_n$ transitions of the $D35^{\bullet+}$ radical cation (compare the difference absorption spectra of $D35^{\bullet+}$ in Fig. 2(B)). In this range, additional weak absorption of injected electrons could be present.[44] Such fast electron injection times of all-organic sensitizers are not unusual and have been observed previously for other systems, *e.g.* alizarin–TiO_2[45] and D149–ZnO.[23] Note that the small spectral dip at around 690 nm might be due to superimposed weak SE of a small fraction of D35 molecules in S_1, which have not yet injected their electrons.

In panel (B), we see an increase of absorption below 515 nm and a decrease of absorption above this wavelength. The band integral for this spectral development stays almost constant. Two time constants of 0.8 ps and 12 ps are obtained for this process from our global analysis of the kinetics. Based on previous time-resolved results for the ultrafast dynamics of the indoline dye D149 on ZnO[23] and PIA spectra of D35 on TiO_2,[6,18,19] we assign this process to a transient Stark effect, originating from the build-up of a local electric field between the $D35^{\bullet+}$ radical cations and injected electrons. This field acts

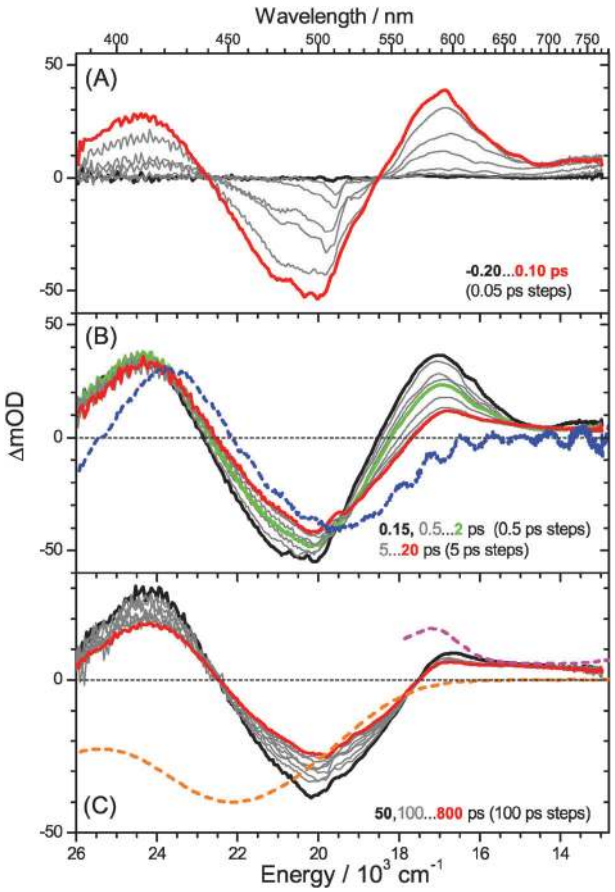

Fig. 6 Transient PSCP spectra of D35 on TiO_2. Laser excitation at 518 nm. The dashed orange line in panel (C) represents a scaled and inverted steady-state absorption spectrum of D35 on TiO_2, and the dashed blue line in panel (B) is its scaled first derivative. The dashed magenta line in panel (C) is the differential absorption spectrum of the $D35^{\bullet+}$ radical cation on TiO_2 from Fig. 2, which was measured down to 560 nm using spectroelectrochemistry.

on the neutral D35 molecules in the ground electronic state S_0, resulting in a blue-shift of the steady-state absorption spectrum. This is also supported by the amplitude ratio 500 nm : 600 nm (bleach/radical cation absorption) in the PSCP spectrum at 20 ps, which is much larger (almost 4 : 1) than that in the difference absorption spectrum obtained from spectroelectrochemistry (only 1.8 : 1, Fig. 2(B)). Note that the Stark field will also act on other species present on the TiO_2 thin film, such as the radical cations, and will certainly influence their spectra to some extent. Note also that the 0.8 ps component might contain a small contribution from the decay of some remaining neutral D35 molecules in S_1 by delayed electron injection. This could explain the disappearance of the small spectral dip at 690 nm in the middle panel. The latter point can only be clarified, if *e.g.* the rise in the radical cation absorption in the near-IR is recorded. This will require an extension of our PSCP setup and will be the subject of a future investigation.

It was previously shown that for the ideal case of aligned dye molecules and electric field lines acting normal to a flat surface, the differential absorption spectrum resulting from a first-order Stark effect should resemble the first derivative of the steady-state absorption spectrum.[20] This derivative is included in panel (B) as a dashed blue line. There is a remarkable similarity between this derivative and the PSCP spectrum at 20 ps (red line), but with three notable differences: (i) the PSCP spectrum is less red-shifted than the derivative spectrum, presumably because the TiO_2 surface structure is far from being ideally flat, and therefore the D35 molecules are not regularly aligned. (ii) There is also an additional absorption above 565 nm, which is not present in the derivative, and this is certainly due to the superimposed absorption of the $D35^{\bullet+}$ radical cation. There are also clear spectral contributions of $D35^{\bullet+}$ in the wavelength region below 440 nm, which give rise to the strong absorption band in that region (compare Fig. 2(B)). (iii) In the derivative of the steady-state absorption spectrum, there is a pronounced undulatory structure arising from interference of the *ca.* 2 μm thick thin film, most clearly visible above 550 nm. This structure is absent in the PSCP spectra. At first sight, this is not surprising because steady-state absorption features of the film should cancel out in a ΔOD measurement. We note, however, that we did observe undulatory structure in PSCP spectra after photoinjection from the indoline dye D149 into electrodeposited ZnO.[23] Undulations in differential absorption spectra arise from changes in the refractive index of the semiconductor oxide thin film due to electron injection.[46] A simple approach based on the Drude model predicts that the change in the refractive index Δn is inversely proportional to the effective electron mass.[47] Because the effective electron mass for TiO_2 is much larger than that for ZnO,[44] the resulting undulations appear to be too weak for detection in the PSCP spectra of the D35–TiO_2 system.

The spectral development up to 800 ps is shown in panel (C) of Fig. 6. The amplitude of the PSCP spectrum decays by about 35% from 50 to 800 ps, and this decay is only present below 650 nm. In contrast, the $D35^{\bullet+}$ absorption above 650 nm remains virtually unchanged. Consequently, the spectral decay cannot arise from electron–cation recombination. Closer inspection reveals that the spectral decay is only observed in the region, which overlaps with the $S_0 \rightarrow S_1$ steady-state absorption, shown as a dashed orange line in (C). It is therefore suggested that this decay arises from a weakening of the local Stark field on longer timescales, as ΔOD_{Stark} is expected to be proportional to the field strength.[20] The reduction of the field strength is likely the result of further diffusion of the injected electrons into the thin film, where at the same time the charge screening by TiO_2 increases. Based on the limited timescale covered in the current experiments, we cannot assign a reliable time constant to this process, but we can estimate a value in the nanosecond range. Certainly, the decay will not progress much further (the spatial electron distribution should reach an equilibrium after some time), as is also supported by previous PIA spectra.[6,18,19]

Selected kinetic traces from the PSCP experiments on TiO_2 are shown in Fig. 5(B) for the same probe wavelengths as in the acetonitrile case (Fig. 5(A)). For D35–TiO_2, the wavelength of 522 nm (red) is located close to an almost isosbestic point of

the biphasic (0.8 ps/11 ps) dynamics of the build-up of the Stark field (Fig. 6(B)). Therefore, one mainly observes immediate formation of GSB and a slow decay which is assigned to the weakening of the Stark field at long times. At 611 nm (green), absorption appears instantaneously and is due to the $D_0 \rightarrow D_n$ transition of $D35^{\bullet+}$, which is formed upon ultrafast electron injection. The pronounced subsequent signal decay is a clear signature of the biphasic Stark dynamics. It arises from increasing bleach, which appears because of the blue-shift of the $S_0 \rightarrow S_1$ absorption band of D35. The subsequent weak decay again arises from the weakening of the electric field at long times. In contrast, the strong absorption of the long-lived $D35^{\bullet+}$ stays constant. The transient at 750 nm (blue) behaves similar to the transient at 611 nm, except for its much smaller total amplitude (less absorption of $D35^{\bullet+}$).

In order to quantify the timescale of the much slower electron–cation recombination, additional experiments were performed on longer timescales employing excitation at 490 nm and probing the recovery of D35 in the GSB band at 532 nm. A representative kinetic trace in the range 10 μs–9 ms is presented in Fig. 7. We observe multiexponential decay characteristics with time constants of *ca.* 30 μs, 170 μs and (much less reliable) 1.4 ms, and a half-life of *ca.* 70 μs. These results can be compared to a previous study, where D35 was excited at 560 nm, with subsequent monitoring of the decay dynamics in the $D35^{\bullet+}$ absorption band at 880 nm (where also weak absorption of conduction band electrons might contribute to the transients).[17] Multiexponential decay behavior was observed in that case, with a half-life of 323 μs for $D35^{\bullet+}$–TiO_2 in contact with an inert electrolyte consisting of 0.1 M $LiClO_4$ and 0.2 M 4-*tert*-butyl-pyridine in acetonitrile. The accelerated recombination in our current experiments can be most likely traced back to the absence of an electrolyte solution at the thin film surface, which results in reduced charge screening. In addition, the higher charge carrier density in the current experiments increases the probability of recombination.

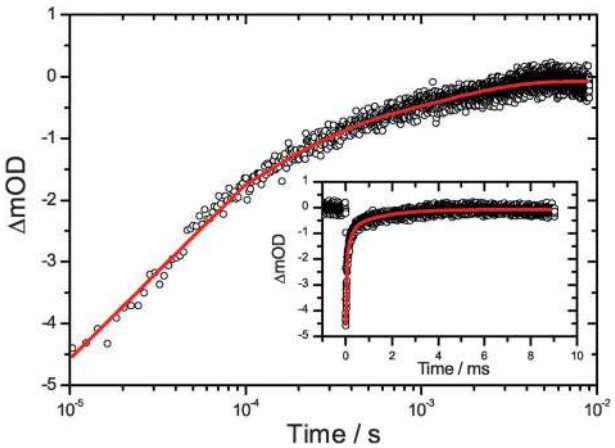

Fig. 7 Transient absorption decay on long timescales for D35 on TiO_2 in contact with air with a logarithmic time axis (inset: linear time axis). λ_{Pump} = 490 nm, λ_{Probe} = 532 nm.

3.5 Transient absorption of D35 on ZrO_2

We have chosen ZrO_2 as a semiconductor oxide with a considerably larger band gap for comparison with the TiO_2 case. Fig. 8 displays transient PSCP spectra for D35–ZrO_2. The spectral development at early times in (A) resembles the initial behavior of D35 on TiO_2 in Fig. 6(A). We therefore assign this partly to the primary charge separation step (within the cross-correlation time of the experiment), presumably forming "closely-bound" electron–cation complexes.[48] Because the conduction band edge of ZrO_2 is located above that of TiO_2,[11,37] one would expect that mostly trap states below the conduction band edge are populated. Note also that no significant stimulated emission (SE) signal is observed in Fig. 8(A) for ZrO_2, which should appear as a negative peak at *ca.* 15 000 cm^{-1} (compare with Fig. 2(A) (magenta)). This supports the interpretation that a substantial fraction of S_1 state population is depleted because "closely-bound" electron–cation complexes are mainly formed. Nevertheless, the spectral "dip" at around 15 000 cm^{-1} (as seen in Fig. 8(B)) is an indication that there must also be superimposed $S_1 \rightarrow S_0$ SE, which is however overwhelmed by the absorption of the electron–cation complexes. The presence of noninjecting D35 molecules in the S_1 state is also reasonable, because there is a clear signal in the steady-state fluorescence spectrum (Fig. 2(A)), which must originate from this fraction of D35 molecules.

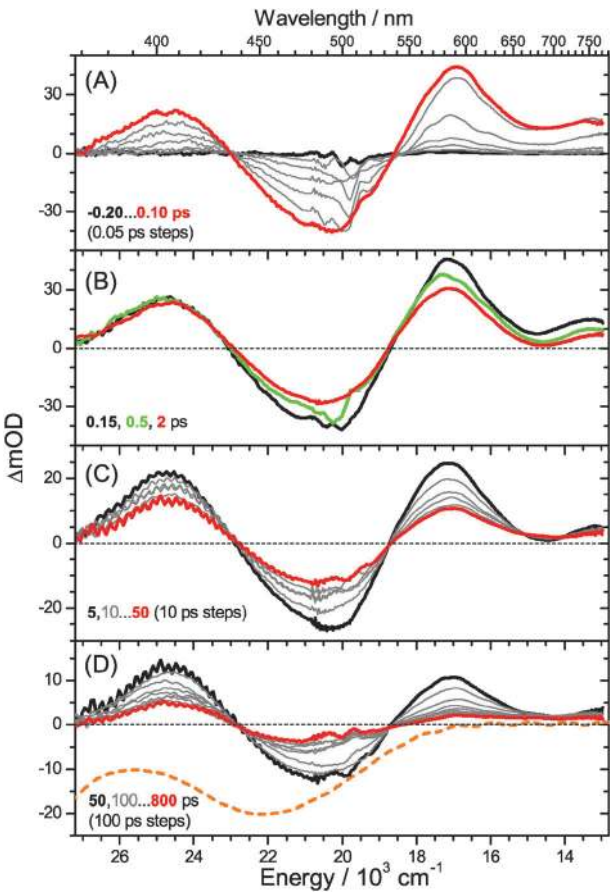

Fig. 8 Transient PSCP spectra of D35 on ZrO_2. Laser excitation at 520 nm.

Significant differences in the spectral development with respect to the TiO_2 case are observed at later times. In neither of the panels Fig. 8(B)–(D) clear signatures of a dynamic Stark shift are observed, in contrast to Fig. 6(B). We take this as an indication that – although to some extent initial charge separation occurs for D35–ZrO_2 – mobile conduction band electrons are hardly formed. In Fig. 8(B), we instead observe a decay of the GSB band at 490 nm and the same holds for the absorption bands below 430 nm and above 530 nm. We assign this to a ''slower'' component of the formation of ''closely-bound'' electron–cation complexes (time constant: *ca.* 0.4 ps). Note that from 0.15 to 2 ps the absorption peak ratio (590 : 400 nm) drops from *ca.* 1.8 : 1 to 1.3 : 1. The latter ratio is similar to the one obtained for D35–TiO_2 immediately after photoexcitation. In addition, relaxation of the complex *e.g.* due to ultrafast intramolecular vibrational redistribution might also contribute to the spectral development in Fig. 8(B).[43]

The development in the remaining two panels, Fig. 8(C) and (D), is dominated by multiexponential decay kinetics. A satisfactory fit is achieved by using time constants of 4, 35 and 550 ps. We assign these dynamics to several processes, which render the dynamics in this system rather complex: charge recombination between trapped electrons and radical cations occurs, where the recombination lifetime strongly depends on the distance of electrons and cations in the complexes: in panel (C), the whole spectrum uniformly decays with the aforementioned 4 and 35 ps time constants, except for the region above 650 nm, where a tiny increase in absorption is observed at around 680 nm. We assign this to a slight spectral narrowing of the absorption spectrum of the electron–cation complex due to vibrational relaxation on a 10–40 ps timescale. An unambiguous determination of the latter value is however not possible, because part of the recombination dynamics also happens on similar timescales. We note that similar vibrational relaxation processes were also observed for other systems, such as $D149^{\bullet+}$ radical cations on ZnO, in that case with a time constant of *ca.* 20 ps, in reasonable agreement with the current observation.[23]

Panel (D) of Fig. 8 highlights the slow decay part (time constant: 550 ps). The residual spectrum (red) has a shape which is very similar to that on TiO_2 at long times (Fig. 6(C)). Therefore we assign this spectral signature to long-lived electron–cation complexes which decay on a nanosecond timescale (not accurately determined in the current experiments). We note that one or several of the aforementioned time constants must also contain contributions from internal conversion of D35 molecules in S_1, which did not inject an electron and are responsible for the fluorescence emission (Fig. 2(A) (magenta line)). Therefore, an accurate determination of the S_1 lifetime of D35 on ZrO_2 is not straightforward. The aforementioned interpretation is further illustrated by the kinetic traces for D35–ZrO_2 in Fig. 5(C). The ultrafast decay at early times is likely due to delayed formation of electron–cation complexes (time constant: 0.4 ps), whereas the multiexponential decays at later times (4, 35, 550 ps), as discussed above, probably arise from recombination within the close electron–cation complexes and superimposed IC of D35 molecules which did not participate in charge separation. Such complex dynamics are not unusual and were reported previously for the system alizarin–ZrO_2.[49]

4. Conclusions

The current transient absorption experiments have provided a comprehensive overview of the photoinduced dynamics of the D35 dye in different environments. In the solvent acetonitrile, D35 exhibits subpicosecond solvation dynamics in response to the substantial change in dipole moment upon photoexcitation to S_1. An additional relaxation process in the S_1 state (possibly some structural relaxation) with a time constant of 7.1 ps is observed, and D35 subsequently decays to S_0 by IC (203 ps). On TiO_2, electron injection into the semiconductor oxide surface dominates, initially forming electron–cation complexes. This process is extremely fast (sub 100 fs, within the time resolution of our experiment). A subsequent biphasic spectral evolution with time constants of 0.8 and 12 ps is assigned to changes in a transient Stark field at the interface (arising from the radical cations and electrons) which acts on D35 molecules in S_0 and shifts their absorption spectrum to the blue. The field will also affect to some extent the spectral properties of other species present at the surface, such as the radical cations. The Stark effect later on slightly weakens on a nanosecond timescale, presumably because of substantial screening of the electrons, as they migrate deeper into the TiO_2. Previous transient absorption experiments for the indoline dye D149 on electrodeposited ZnO also found similar transient dynamics with similar spectral signatures, however with a slower time constant of *ca.* 20 ps. This was also assigned to a local Stark effect.[23] For D149–ZnO, no indication for even a partial decay of the Stark features was seen up to 800 ps. Additional studies will be therefore required to fully understand the contributions of different physical processes to the transient shift of the Stark features. The transient local Stark effect will be influenced by factors such as *e.g.* the timescale of dissociation of the initially formed electron–cation complexes, diffusion timescales of mobile electrons, reorientational motion of D35 molecules in S_0 in response to changes in the electric field and spectral shifts of neutral sensitizer molecules induced by the radical cations remaining on the surface after electron injection. To reach this goal, systematic experimental studies of *e.g.* a stable reference dye on ZnO and TiO_2 in different environments (air, solvent with an electrolyte and with or without a redox system) over a wide spectral range are required. In any case, the current results for D35–TiO_2 and also previous ones for D149–ZnO highlight the importance to include such transient spectral effects, which arise from the build-up of interfacial electric fields, in the interpretation of the (sub)picosecond dynamics in pump–probe absorption spectra of sensitizer dyes on thin mesoporous semiconductor oxide films.

Acknowledgements

We would like to thank N. P. Ernsting, J. L. Pérez Lustres, J. Lange and A. Müller for their help during the implementation

of the PSCP setup, J. Troe and A. M. Wodtke for ongoing support, and R. Oswald for technical assistance during the calculations. We thank M. Adlung and C. Wickleder for providing the programmable oven for TiO_2 and ZrO_2 film sintering. In addition, we acknowledge excellent technical support from D. Gaumann, B. Meyer and M. Rabe in Siegen. This work was supported by the Priority Programme SPP 1191 ''Ionic Liquids'' of the German Research Foundation. P. W. Lohse also would like to thank for the funding from the European Community's Seventh Framework Programme (FP7/2007-13) under grant agreement no. 246124 of the SANS project.

Notes and references

1 A. Hagfeldt, G. Boschloo, L. Sun, L. Kloo and H. Pettersson, *Chem. Rev.*, 2010, **110**, 6595.
2 T. Kitamura, M. Ikeda, K. Shigaki, T. Inoue, N. A. Anderson, X. Ai, T. Lian and S. Yanagida, *Chem. Mater.*, 2004, **16**, 1806.
3 D. P. Hagberg, T. Edvinsson, T. Marinado, G. Boschloo, A. Hagfeldt and L. Sun, *Chem. Commun.*, 2006, 2245.
4 D. P. Hagberg, J.-H. Yum, H. Lee, F. De Angelis, T. Marinado, K. M. Karlsson, R. Humphry-Baker, L. Sun, A. Hagfeldt, M. Grätzel and M. K. Nazeeruddin, *J. Am. Chem. Soc.*, 2008, **130**, 6259.
5 K. R. J. Thomas, Y.-C. Hsu, J. T. Lin, K.-M. Lee, K.-C. Ho, C.-H. Lai, Y.-M. Cheng and P.-T. Chou, *Chem. Mater.*, 2008, **20**, 1830.
6 S. M. Feldt, E. A. Gibson, E. Gabrielsson, L. Sun, G. Boschloo and A. Hagfeldt, *J. Am. Chem. Soc.*, 2010, **132**, 16714.
7 D. P. Hagberg, X. Jiang, E. Gabrielsson, M. Linder, T. Marinado, T. Brinck, A. Hagfeldt and L. Sun, *J. Mater. Chem.*, 2009, **19**, 7232.
8 J. Wiberg, T. Marinado, D. P. Hagberg, L. Sun, A. Hagfeldt and B. Albinsson, *J. Phys. Chem. B*, 2010, **114**, 14358.
9 X. Jiang, K. M. Karlsson, E. Gabrielsson, E. M. J. Johansson, M. Quintana, M. Karlsson, L. Sun, G. Boschloo and A. Hagfeldt, *Adv. Funct. Mater.*, 2011, **21**, 2944.
10 H. N. Tsao, C. Yi, T. Moehl, J.-H. Yum, S. M. Zakeeruddin, M. K. Nazeeruddin and M. Grätzel, *ChemSusChem*, 2011, **4**, 591.
11 C. Martín, M. Ziólek, M. Marchena and A. Douhal, *J. Phys. Chem. C*, 2011, **115**, 23183.
12 J.-H. Yum, E. Baranoff, F. Kessler, T. Moehl, S. Ahmad, T. Bessho, A. Marchioro, E. Ghadiri, J.-E. Moser, C. Yi, M. K. Nazeeruddin and M. Grätzel, *Nature*, 2012, **3**, 631.
13 M. Ziolek, I. Tacchini, M. T. Martínez, X. Yang, L. Sun and A. Douhal, *Phys. Chem. Chem. Phys.*, 2011, **13**, 4032.
14 M. Ziolek, B. Cohen, X. Yang, L. Sun, M. Paulose, O. K. Varghese, C. A. Grimes and A. Douhal, *Phys. Chem. Chem. Phys.*, 2012, **14**, 2816.
15 S. Haid, M. Marszalek, A. Mishra, M. Wielopolski, J. Teuscher, J.-E. Moser, R. Humphry-Baker, S. M. Zakeeruddin, M. Grätzel and P. Bäuerle, *Adv. Funct. Mater.*, 2012, **22**, 1291.
16 X. Jiang, T. Marinado, E. Gabrielsson, D. P. Hagberg, L. Sun and A. Hagfeldt, *J. Phys. Chem. C*, 2010, **114**, 2799.
17 S. M. Feldt, G. Wang, G. Boschloo and A. Hagfeldt, *J. Phys. Chem. C*, 2011, **115**, 21500.
18 L. Yang, U. B. Cappel, E. L. Unger, M. Karlsson, K. M. Karlsson, E. Gabrielsson, L. Sun, G. Boschloo, A. Hagfeldt and E. M. J. Johansson, *Phys. Chem. Chem. Phys.*, 2012, **14**, 779.
19 Z. Yu, H. Tian, E. Gabrielsson, G. Boschloo, M. Gorlov, L. Sun and L. Kloo, *RSC Adv.*, 2012, **2**, 1083.
20 U. B. Cappel, S. M. Feldt, J. Schöneboom, A. Hagfeldt and G. Boschloo, *J. Am. Chem. Soc.*, 2010, **132**, 9096.
21 S. Ardo, Y. Sun, A. Staniszewski, F. N. Castellano and G. J. Meyer, *J. Am. Chem. Soc.*, 2010, **132**, 6696.
22 S. Ardo, Y. Sun, F. N. Castellano and G. J. Meyer, *J. Phys. Chem. B*, 2010, **114**, 14596.
23 K. Oum, P. W. Lohse, O. Flender, J. R. Klein, M. Scholz, T. Lenzer, J. Du and T. Oekermann, *Phys. Chem. Chem. Phys.*, 2012, **14**, 15429.
24 A. L. Dobryakov, S. A. Kovalenko, A. Weigel, J. L. Pérez Lustres, J. Lange, A. Müller and N. P. Ernsting, *Rev. Sci. Instrum.*, 2010, **81**, 113106.
25 P. W. Lohse, J. Kuhnt, S. I. Druzhinin, M. Scholz, M. Ekimova, T. Oekermann, T. Lenzer and K. Oum, *Phys. Chem. Chem. Phys.*, 2011, **13**, 19632.
26 K. Golibrzuch, F. Ehlers, M. Scholz, R. Oswald, T. Lenzer, K. Oum, H. Kim and S. Koo, *Phys. Chem. Chem. Phys.*, 2011, **13**, 6340.
27 T. Lenzer, S. Schubert, F. Ehlers, P. W. Lohse, M. Scholz and K. Oum, *Arch. Biochem. Biophys.*, 2009, **483**, 213.
28 M. Krejcik, M. Danek and F. Hartl, *J. Electroanal. Chem.*, 1991, **317**, 179.
29 U. B. Cappel, E. A. Gibson, A. Hagfeldt and G. Boschloo, *J. Phys. Chem. C*, 2009, **113**, 6275.
30 A. D. Becke, *J. Chem. Phys.*, 1993, **98**, 5648.
31 E. Runge and E. K. U. Gross, *Phys. Rev. Lett.*, 1984, **52**, 997.
32 A. Dreuw and M. Head-Gordon, *Chem. Rev.*, 2005, **105**, 4009.
33 M. Pastore, E. Mosconi, F. De Angelis and M. Grätzel, *J. Phys. Chem. C*, 2010, **114**, 7205.
34 M. J. Frisch, G. W. Trucks, H. B. Schlegel and G. E. Scuseria, *et al.*, *Gaussian 09, Revision A.01*, Gaussian, Inc., Wallingford, CT (USA), 2009.
35 M. Head-Gordon, A. M. Grana, D. Maurice and C. A. White, *J. Phys. Chem.*, 1995, **99**, 14261.
36 Y. Shao, L. Fusti-Molnar, Y. Jung and J. Kussmann, *et al.*, *Phys. Chem. Chem. Phys.*, 2006, **8**, 3172.
37 B. I. Lemon, F. Liu and J. T. Hupp, *Coord. Chem. Rev.*, 2004, **248**, 1225.
38 M. L. Horng, J. A. Gardecki, A. Papazyan and M. Maroncelli, *J. Phys. Chem.*, 1995, **99**, 17311.
39 J. L. Pérez Lustres, S. A. Kovalenko, M. Mosquera, T. Senyushkina, W. Flasche and N. P. Ernsting, *Angew. Chem., Int. Ed.*, 2005, **44**, 5635.
40 M. Sajadi, M. Weinberger, H.-A. Wagenknecht and N. P. Ernsting, *Phys. Chem. Chem. Phys.*, 2011, **13**, 17768.
41 M. Zuleta, T. Edvinsson, S. Yu, S. Ahmadi, G. Boschloo, M. Göthelid and A. Hagfeldt, *Phys. Chem. Chem. Phys.*, 2012, **14**, 10780.
42 K. Oum, P. W. Lohse, F. Ehlers, M. Scholz, M. Kopczynski and T. Lenzer, *Angew. Chem., Int. Ed.*, 2010, **49**, 2230.

43 T. Lenzer, F. Ehlers, M. Scholz, R. Oswald and K. Oum, *Phys. Chem. Chem. Phys.*, 2010, **12**, 8832.
44 B. Enright and D. Fitzmaurice, *J. Phys. Chem.*, 1996, **100**, 1027.
45 R. Huber, J.-E. Moser, M. Grätzel and J. Wachtveitl, *J. Phys. Chem. B*, 2002, **106**, 6494.
46 C. Bauer, G. Boschloo, E. Mukhtar and A. Hagfeldt, *Chem. Phys. Lett.*, 2004, **387**, 176.
47 N. Guijarro, Q. Shen, S. Giménez, I. Mora-Seró, J. Bisquert, T. Lana-Villarreal, T. Toyoda and R. Gómez, *J. Phys. Chem. C*, 2010, **114**, 22352.
48 H. Nemec, J. Rochford, O. Taratula, E. Galoppini, P. Kuzel, T. Polívka, A. Yartsev and V. Sundström, *Phys. Rev. Lett.*, 2010, **104**, 197401.
49 R. Huber, S. Spörlein, J. E. Moser, M. Grätzel and J. Wachtveitl, *J. Phys. Chem. B*, 2000, **104**, 8995.

